PCCP

PAPER

View Article Online
View Journal | View Issue

Cite this: *Phys. Chem. Chem. Phys.*, 2014, **16**, 18765

Simple cathode design for Li–S batteries: cell performance and mechanistic insights by in operando X-ray diffraction†

Jörn Kulisch,[ab] Heino Sommer,[ab] Torsten Brezesinski*[a] and Jürgen Janek*[ac]

Received 21st May 2014,
Accepted 22nd July 2014

DOI: 10.1039/c4cp02220c

www.rsc.org/pccp

Rechargeable batteries have been receiving increasing attention over the past several years, particularly with regard to the accelerated development of electric vehicles, but also for their potential in grid storage applications. Among the broad range of cathode active materials, elemental sulfur has the highest theoretical specific capacity, thereby making it one of the most promising positive electrode materials these days. In the present work, we show that already a simple cathode design (cathodes with a non-optimized composite microstructure) provides good electrochemical performance both in coin and pouch cells with sulfur loadings of 2 mg cm^{-2}. Our research data demonstrate that (1) specific capacities of 1000 mA h g^{-1} can be achieved over 60 cycles at room temperature while the cyclability at elevated temperatures (here, $\vartheta > 40$ °C) is poor, (2) the discharge is the kinetically rate-limiting process, (3) the major fraction of active sulfur in the electrode is lost during the formation cycle at C/50 and (4) the Li–S cells suffer from drying-out due to continuous electrolyte decomposition on the lithium metal anode. In addition, *in operando* X-ray diffraction shows Li_2S formation (grain size of <10 nm) on discharge and the appearance of single phase β-sulfur in the sub-100 nm size range – rather than the thermodynamically stable orthorhombic polymorph (α-sulfur) – by the end of the charge cycle.

1. Introduction

The lithium–sulfur (Li–S) technology is one of the most active research areas in the field of electrochemical energy storage. Sulfur as active cathode material has a high theoretical specific capacity of 1672 mA h g^{-1}, thereby demanding an anode with a similar capacity to achieve the highest possible energy density on cell level. Up until now, only lithium meets this requirement, while providing an average voltage of 2.2 V for the Li–S battery system.[1–6] On the basis of these numbers and assuming full conversion of sulfur to lithium sulfide (Li_2S) by transfer of 16 electrons during the electrochemical reduction process, a theoretical energy density of ~2600 W h kg^{-1} can, in principle, be achieved. This value is five times the theoretical energy density of well-established half-cell couples such as $LiCoO_2$/graphite. However, practical energy densities of lithium-ion batteries are currently only in the range of 100–200 W h kg^{-1}, which illustrates the loss of capacity in developing the functioning battery from the mere redox couples.[2,7,8]

Besides the high theoretical energy density, the use of sulfur for the development of next-generation lithium batteries is also desirable as it is an abundant, low cost material that is environmentally sustainable. Nevertheless, there are several issues related to safety and cycling stability to overcome before the Li–S technology becomes viable for commercial application. For example, deleterious side reactions such as the continuous electrolyte decomposition on the lithium metal anode and dissolution of reactive intermediates lead to severe capacity fading during cycling.[3,9–11] As for the latter issue, lithium polysulfides of different solubility and chain lengths are formed at the cathode side upon discharging/charging the cell. Driven by a concentration gradient, the higher-order polysulfides diffuse to the anode, where they react with the lithium to generate lower-order polysulfides, which then diffuse back to the cathode to form again long-chain lithium polysulfides. This so-called shuttle mechanism inevitably results in both a fairly high self-discharge rate and low coulombic efficiencies. In addition, it causes loss of active material, *e.g.*, through formation of insoluble and electrically insulating Li_2S at the anode.[6,9–11]

Many approaches to addressing the problem of a quasi-liquid cathode have been reported in the literature. Apart from

[a] *Battery and Electrochemistry Laboratory, Institute of Nanotechnology, Karlsruhe Institute of Technology, Hermann-von-Helmholtz-Platz 1, 76344 Eggenstein-Leopoldshafen, Germany. E-mail: torsten.brezesinski@kit.edu, juergen.janek@kit.edu*
[b] *BASF SE, 67056 Ludwigshafen, Germany*
[c] *Institute of Physical Chemistry, Justus-Liebig-University Giessen, Heinrich-Buff-Ring 58, 35392 Giessen, Germany*

† Electronic supplementary information (ESI) available: Additional data from SEM imaging and galvanostatic cycling. See DOI: 10.1039/c4cp02220c

adding adsorptive agents, the use of nanostructured materials to trap the generated polysulfides in the cathode architecture seems to provide a viable solution to the problem.[12–15] Predominantly porous carbons with different morphologies, including nanotubes, particles and fibers, to mention only a few, have been tested so far.[16–25] However, other materials such as hollow spheres of amorphous titanium dioxide and functionalized polymers turned out to be promising as well.[5,26–28] Nevertheless, it is important to note that in the majority of these publications the sulfur loading, and thus also the areal capacity was comparably low (less than or equal to $\sim$1 mA h cm^{-2}). Both the sulfur content in the final electrode and the mass loading strongly affect the overall performance of the Li–S cells. Therefore, in our opinion, it is still inconclusive whether advanced nanocomposite cathodes are needed at all to increase the lifetime of such cells.[29] Also, a direct comparison of different Li–S systems seems difficult, because several key parameters such as the electrode composition and processing often differ significantly among the cathodes that have been described in the literature.

The most common electrolyte for Li–S batteries consists of a mixture of 1,2-dioxolane (DOL), 1,2-dimethoxyethane (DME) and lithium bis(trifluoromethanesulfonyl)imide (LiTFSI). In addition, a certain amount of lithium nitrate is typically added, with which the polysulfide shuttle can be suppressed – lithium nitrate has been shown to be an effective solid electrolyte interface (SEI) forming agent in combination with the ether-based solvents.[3,9,30–33] The stability of the electrolyte components against lithium and their ability to form a stable SEI are crucial to prevent unfavorable side reactions at the anode, *that is*, for the working principle in general. Consequently, the issue of anode protection is gaining more attention in the community than ever.

In this paper, we show that a simple cathode design, including only non-tailor-made materials (namely, commercially available carbon blacks, micron-sized sulfur and a poly(vinyl alcohol) polymer binder),[34] offers a good electrochemical performance both in coin-type and pouch cells. Such Li–S cells are competitive in various ways with the many batteries using nanostructured sulfur composite electrodes. Overall, our research goal was two-fold: first, to fabricate standardized electrodes with a reasonable sulfur loading as a kind of reference system and second, to study the cell chemistry and quantify the performance limitations imposed by the structural simplicity of the cathode architecture.

2. Experimental

Electrode processing and materials

For the preparation of the cathodes, sulfur (Aldrich, reagent grade), Super C65 (Timcal) and Printex XE2 (Orion) in a ratio of 3.4 : 1 : 1 were ground. Poly(vinyl alcohol) Selvol 425 (Sekisui) dissolved in a mixed solvent of water and isopropanol was subsequently added to the blend.[35–37] The resulting mixture was ball-milled for 20 h to form a homogeneous slurry. The slurry was then coated onto 8 μm-thick primed aluminum (containing 2/3 Super C65 and 1/3 Selvol 425) with a doctor blade and dried in vacuum at 40 °C for 16 h.[38] The sulfur content in the final electrode was about 60% and sulfur loadings of 1.7–2.3 mg cm^{-2} were obtained (determined by weighing the electrodes before and after coating and knowing the nominal composition). We estimate the error margin as being $\pm$2%.

Coin-type cells were assembled in an argon-filled glovebox using a polyethylene separator (Celgard EK2040) and lithium foil (China Lithium Ltd., 600 μm) as negative electrode. For pouch cells, the assembling was performed in a dry room by stacking the lithium foil (Chemetall Foote Corp., 50 μm), separator and cathode. The electrolyte used was a solution of 8 wt% lithium bis(trifluoromethanesulfonyl)imide (Aldrich, 99.95%), 4 wt% lithium nitrate (Merck, 99.995%), 44 wt% 1,2-dimethoxyethane (Alfa Aesar, 99+%) and 44 wt% 1,3-dioxolane (Acros, 99.8%). Prior to use, the solid electrolyte components were dried in vacuum and the solvents were purified by distillation from sodium potassium alloy under argon. The water content in the electrolyte was as low as 33 ppm, as determined by Karl-Fischer titration.

Electrochemical testing

Galvanostatic charge–discharge measurements were carried out in a potential range between 1.7 V and 2.5 V *vs.* Li/Li$^+$ using a MACCOR (Tulsa, Oklahoma) battery cycler. After 1 cycle at C/50 (with 1C = 1672 mA $g_{(S)}{}^{-1}$) was completed, the cells were cycled at charge and discharge rates of C/8 and C/5, respectively. Part of the reason for this is that at such C-rates, high specific capacities can be achieved while keeping the cell failure rate at a minimum. All electrochemical experiments were conducted under stable environmental conditions in a BINDER cooled incubator. The electrolyte-to-sulfur mass ratios were 20 : 1 and 10 : 1 for coin-type and pouch cells, respectively.

Methods

Field-emission scanning electron microscopy (SEM) images were recorded with a LEO 1530 instrument at 10 kV. *In operando* X-ray diffraction (XRD) measurements were carried out at the Synchrotron Light Source ANKA on the PDIFF beamline (wavelength of 0.08856 nm, beam size of 1.5 mm (vertical) $\times$ 0.25 mm (horizontal), sample-to-detector distance of 215.402 mm) using a Pilatus 300k detector (counting time of 30 s).

3. Results

The cathodes studied in the present work were obtained by simply mixing two commercially available carbon blacks and sulfur with a water-soluble poly(vinyl alcohol) binder.[34] The latter was chosen to avoid the harsh drying conditions – and the associated potential loss of sulfur from the electrode – required when using a non-water-soluble polymer binder such as poly(vinylidene fluoride). Overall, the preparation procedure is not only straightforward, but also yields high quality electrodes with few cracks, as can be seen from the top view and cross-sectional SEM images in Fig. 1 (see also SEM images at different magnifications in Fig. S1 of the ESI†).

Cathodes with sulfur loadings of 2 mg cm^{-2} on average were tested in coin-type cells against lithium foil. However, electrochemical measurements were also conducted on 5 $\times$ 5 cm^2

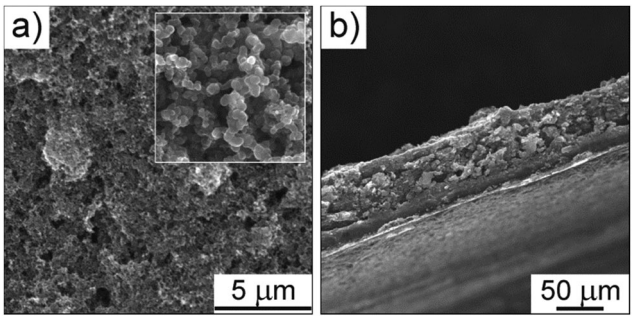

Fig. 1 (a) Top view and cross-sectional (b) SEM images of a non-calendered, ~45 μm-thick sulfur cathode on primed aluminum before galvanostatic cycling, showing the electrode is porous and the top surface is largely crack-free on the micrometer-length scale. The side length of the high-magnification image in the inset of panel (a) is 1.1 μm.

pouch cells to gain insight into the scalability behavior. Fig. 2a shows both the specific discharge and charge capacities and the coulombic efficiency as a function of cycle number for a Li–S cell that was cycled at 25 °C. As is evident from these data, a stable specific capacity of ~1000 mA h g^{-1}, corresponding to an areal capacity of ~2 mA h cm^{-2}, can be achieved over 60 cycles at a discharge rate of C/5. After the first few cycles, the coulombic efficiency, which is defined as the ratio between the discharge capacity and the previous charge capacity, stabilizes above 99%. This result demonstrates that the shuttle mechanism is, in fact, effectively suppressed through the use of lithium nitrate as an additive in the electrolyte. The capacity begins to fade almost linearly after 60 cycles. This fading is associated with a non-negligible increase in polarization. Representative voltage–capacity curves are given in Fig. 2b, showing the typical discharge plateaus for the Li–S system at 2.35 V and 2.1 V *versus* Li/Li^+.

Through a large number of experiments with our standardized cathode we found out that both the amount of electrolyte and the cell design strongly affect the overall performance of the Li–S batteries. As mentioned in the experimental section, we used an electrolyte-to-sulfur mass ratio of 20 : 1 for the coin-type cell experiments. It should be emphasized, nevertheless, that a ratio of smaller than 5 : 1 is needed to achieve competitive energy densities. From the 60th cycle onwards we see a steady increase in overpotential (relative to lithium), which is indicated by the decrease in mean discharge voltage (see voltage profiles in Fig. 2b). We presume that this is mainly due to the fact that the cells start to dry out because the electrolyte is irreversibly consumed during the course of cycling. This hypothesis is confirmed to some extent by post mortem analysis of different cells. The vast majority seemed rather dry once they have run for 100 cycles. Another indication of continuous electrolyte decomposition is that the lithium metal shows a mossy, grey surface, thereby suggesting uneven deposition of highly reactive lithium upon charging. Similar results were also obtained from the post mortem analysis of pouch cells. This kind of cells is much closer to potential commercial ones with regard to design, dead volume and other parameters. Overall, the data discussed in this section demonstrate that the amount of both

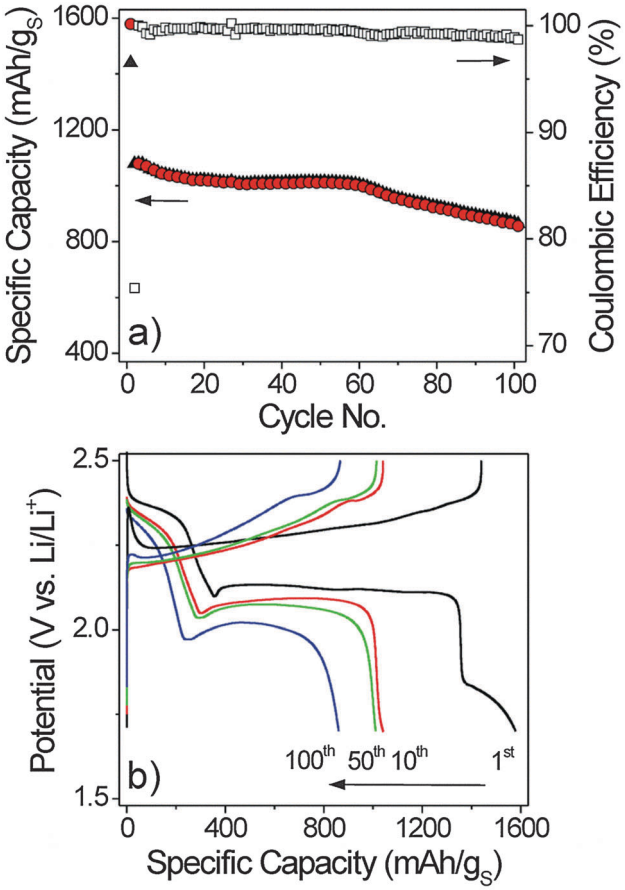

Fig. 2 Cycling performance of the Li–S cells at 25 °C. The 1st cycle was performed at C/50. Thereafter, discharge and charge current rates of C/5 and C/8, respectively, were used. (a) Specific capacity and coulombic efficiency *versus* cycle number. The charge and discharge capacities are shown as black triangles and red circles, respectively. (b) Voltage–capacity curves for the 1st (black), 10th (red), 50th (green) and 100th (blue) cycles.

electrolyte and active mass has to be taken into account when analyzing and comparing the performance of different types of Li–S batteries, and further indicate that drying-out effects have a significant impact on the cycling stability – they seem to limit the overall lifetime of the cells.[29,39]

The electrochemical performance of the Li–S cells at temperatures above 25 °C was analyzed by galvanostatic cycling as well. From Fig. 3 it is apparent that they can be cycled at 40 °C with a slightly faster capacity fading in the first 60 cycles. Thereafter, the fading is more pronounced to that observed at 25 °C. In contrast, cells running at 60 °C show severe fading right from the beginning; the drop-off in specific capacity levels off after about 80 cycles. Analysis of the 1st discharge–charge cycle, which is often referred to as formation cycle and typically conducted at low current rates (here, C/50), provides similar specific capacities for the measurements at 25 °C and 40 °C. However, the capacities on the subsequent cycles are lower by ~100 mA h g^{-1} at 40 °C, as compared to 25 °C. Furthermore, it can be seen that the coulombic efficiency values show more scatter, but also stabilize above 99% after 3 cycles. The coulombic

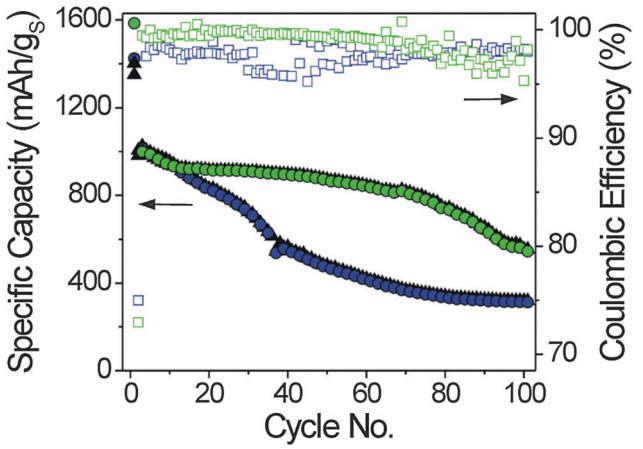

Fig. 3 Cycling performance of the Li–S cells at 40 °C (green) and 60 °C (blue). After the formation cycle at C/50, the discharge and charge current rates were increased to C/5 and C/8, respectively. Both the specific charge (black triangles) and discharge (colored circles) capacities and the coulombic efficiencies are shown.

efficiency of the Li–S cell cycled at 60 °C is in the range of 95–99%. The capacity retention after 100 cycles based on the second cycle discharge capacity, *that is*, after the formation cycle, is 80%, 54% and 31% at 25 °C, 40 °C and 60 °C, respectively. Our studies thus show that the performance at elevated temperatures is rather poor which, we believe, is due to both an accelerated degradation of the electrolyte associated with the destabilization of the (already unstable) SEI on lithium and a more severe leaching of active material from the cathode because of the higher solubility of the different sulfur species and the faster reaction kinetics (see also 1st and 2nd cycle discharge profiles in Fig. S2 of the ESI†). The reduction rate of the polysulfides to insoluble Li_2S at the anode is assumed to be accelerated as well. Therefore, just as for conventional Li-ion batteries, the temperature has a profound effect on the cell performance.[40] Overall, the data in Fig. 3 lead us to conclude that the system studied here provides a "stable" performance only at temperatures below 40 °C and specific measures have to be taken to achieve reliable and durable Li–S batteries at temperature higher than 25 °C.

In the ensuing section we take a closer look at the 1st cycle as well as the room temperature discharge/charge kinetics of the Li–S cells. As previously mentioned, the so-called formation cycle was performed at a rate of C/50. Such a low C-rate is found to be crucial to achieving a "stable" performance in the subsequent cycles. Possible explanations are that low C-rates during the first discharge/charge of the cell (1) ensure virtually complete sulfur utilization and (2) facilitate a more homogeneous distribution of the active material in the cathode (after charging the cell). A uniform distribution of the electronically and ionically insulating micron-sized sulfur particles can probably not be achieved by the electrode processing itself. In this context, we note that the nanocomposite cathodes (S@CMK-3, S@TiO_2, S@CHS and others) mentioned above in the introduction to this article showed a sulfur utilization of 70% or less in the initial cycles, which is comparably low. There are only few examples described in the literature, where a specific capacity close to the theoretical value of 1672 mA h g^{-1} was achieved in the first discharge. Nevertheless, also these cathodes delivered specific capacities of less than 1000 mA h g^{-1} in the subsequent cycles. However, we emphasize again that a direct comparison of the Li–S system employed in this work to others is very difficult because of the different cathode composition (the sulfur content is often much lower than 60%), loading, cycling conditions *etc.*

Furthermore, it can be seen from the data in Fig. 2 and 3 that the loss of active material in the 1st cycle or, in other words, the loss in specific capacity during discharging/charging a fresh cell is significant. To gain more insight into this phenomenon, measurements were carried out with discharge and charge current rates of C/50 at different stages of the cycling process (see Fig. S3 of the ESI†). We found that when the first 2 cycles are performed at C/50, the specific discharge capacity decreases by 13% from 1484 mA h g^{-1} to 1295 mA h g^{-1}. Similarly, when the 1st and 12th cycles are performed at C/50 (2nd–11th cycles at C/5), the loss in specific capacity is ~15%. Since both values are in fair agreement with each other, we conclude that the major fraction of the active sulfur in the electrode is lost during the formation cycle. Overall, the loss appears to be similar for different high quality electrodes (at similar electrolyte-to-sulfur mass ratios), which implies that this is an intrinsic issue of Li–S batteries.

The rate performance of the Li–S cells was measured by increasing the discharge current from C/5 to 1C while maintaining the charge current at a rate of C/8 during each cycle (see Fig. 4a). The same experiment was also carried out with different C-rates on charging while keeping the discharge current fixed at C/5 (see Fig. 4b). As is evident, the discharge capacity decreases by almost 80% from 1000 mA h g^{-1} at C/5 to ~200 mA h g^{-1} at 1C. Also, the coulombic efficiency is lower than 99% at the highest C-rate (here, 1C). In contrast, the impact of the charge current rate on both the specific capacity and the coulombic efficiency is much less significant; ~60% of the second cycle capacity is retained at 1C. Therefore, the data in Fig. 4 demonstrate that the discharge (lithiation) is the rate-limiting process from the kinetic point of view. However, it can also be seen that the Li–S cells are capable of delivering a reversible specific capacity of ~850 mA h g^{-1} at C/2. Considering the electrode composition and sulfur loading, this value is promising. Nevertheless, the kinetic limitations are more pronounced than in nanocomposite electrodes with optimized microstructure. For example, recent work has shown that the discharge/charge kinetics of Li–S cells with a similar or even higher mass loading can be enhanced by reducing the sulfur particle size from the micrometer scale to the nanometer level and embedding the sulfur in a conductive carbon matrix.[41] Such electrode architectures may provide a lower electrical resistance throughout the bulk of the electrode and shorter diffusion path lengths for electron and lithium ion transport.

Lastly, to better understand the cell chemistry, a series of synchrotron-based *in operando* XRD measurements in transmission mode was carried out. We are aware of only a few such studies on Li–S cells up to date.[42–44] Representative XRD data in

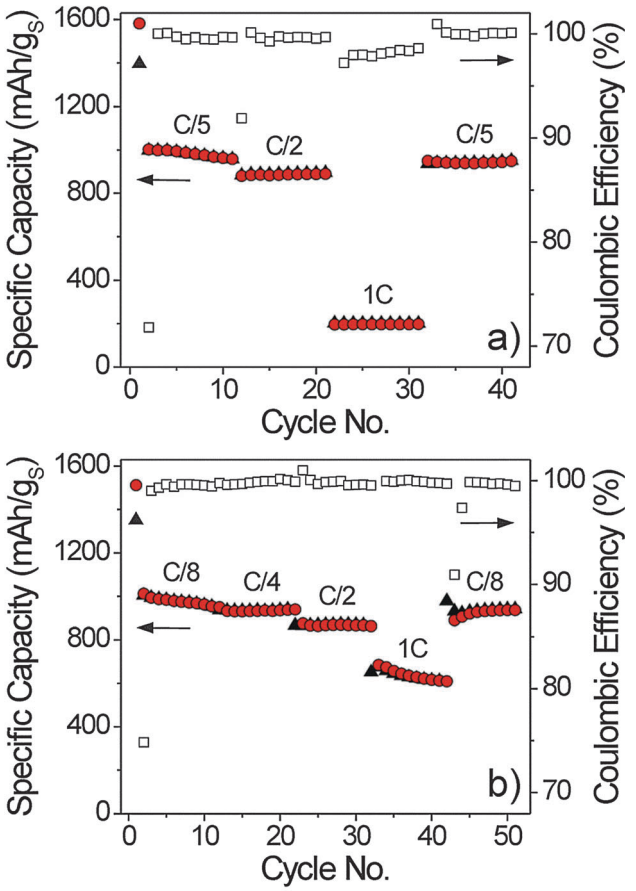

Fig. 4 Specific charge (black triangles) and discharge (red circles) capacities and coulombic efficiency *versus* cycle number for different C-rates. (a) The discharge current was increased from C/5 to 1C while maintaining the charge current rate at C/8. (b) The charge current was increased from C/8 to 1C while keeping the discharge current rate constant at C/5. Note that the rate performance was measured after 1 cycle at C/50 was completed.

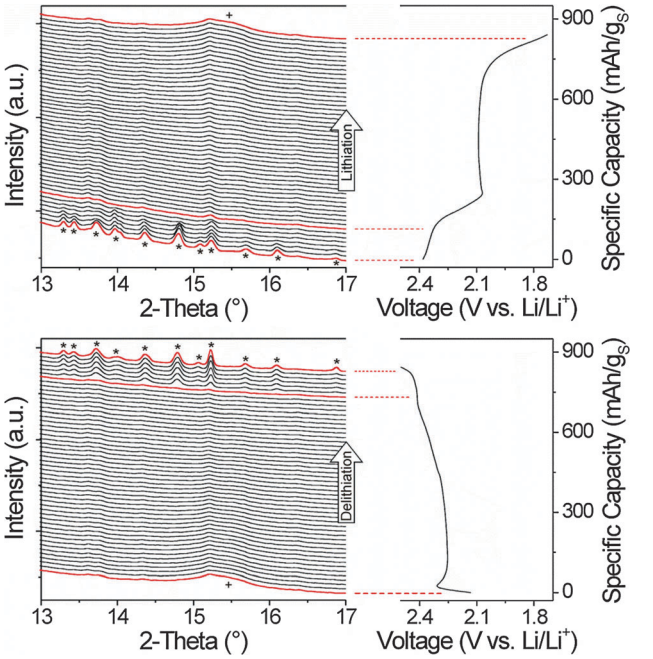

Fig. 5 Synchrotron-based *in operando* XRD data (λ = 0.08856 nm) obtained on a Li–S pouch cell cycled at C/5 (5th cycle). Cubic Li_2S and monoclinic β-sulfur indicated by the plus and asterisk marks, respectively, can be clearly observed. The corresponding voltage profiles are shown on the right.

the range of 2θ from 13° to 17°, recorded during a full discharge–charge cycle at a rate of C/5, are shown in Fig. 5. Our studies establish that (1) the discharge process leads to the formation of cubic Li_2S with sub-10 nm diameter crystallites and (2) single phase β-sulfur in the space group $P2_1/c$ (C_{2h}^5) appears by the end of the charge cycle. Overall, these results are consistent with those of Walus *et al.*,[42] but differ from the data reported by Nelson *et al.*[43] As can be seen from the XRD patterns, the peaks corresponding to monoclinic β-sulfur diminish with increasing lithiation and eventually disappear by the end of the first discharge plateau. This means that all of the active (and crystalline) sulfur is converted to higher- and lower-order lithium polysulfides. Apart from the peaks of other cell components, the subsequent patterns are featureless. It is difficult to tell from the data at which potential the formation of nanocrystalline Li_2S occurs because the (111) peak at 15.5° is broad and comparably weak in intensity. Nevertheless, it seems that this compound is, in fact, present with the beginning of the second discharge plateau, as shown by Walus *et al.*[42]

Similar results were obtained during charging the Li–S cell. Cubic Li_2S disappears when the state of charge (SOC) is above 70% and polycrystalline β-sulfur in phase pure form reappears at about 85% SOC.

XRD patterns obtained at the end of the 5th discharge and charge cycles with the corresponding peak indexing are shown in Fig. 6 (the Joint Committee on Powder Diffraction Standards reference card used for β-sulfur was: no. 34-0941). At first

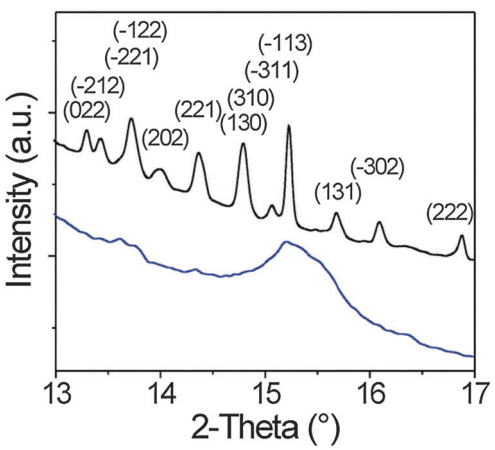

Fig. 6 Synchrotron-based XRD data (λ = 0.08856 nm) obtained at the end of the 5th discharge (blue line) and charge (black line) cycles. Peaks for monoclinic β-sulfur are indexed. The different full width at half maximum intensities indicate anisotropic crystal growth. The fact that the peak at a 2θ of ~15.5° (blue line) is much broader than those of β-sulfur is due to the lower degree of crystallinity of the Li_2S.

glance, the formation of the high temperature β-phase rather than the thermodynamically stable α-sulfur is unusual, but seems to be of a more general nature. However, the reason for this is not yet fully understood. The average crystallite size was determined by applying the Scherrer equation to the line broadening of the rather symmetric (–311) and (–113) peaks. This analysis provides values in the range of 80–90 nm. In addition, it can be seen that some peaks are much broader, thereby implying that the crystallites are anisotropic in shape. Furthermore, we find that the peaks are slightly shifted from the equilibrium spacings (here, towards higher angles), which might be due to strain in the lattice (*e.g.*, Laplace pressure from being a nanoscale material).

Future work in this direction will be aimed at investigating whether the cathode architecture and kinetic effects, including temperature, affect the β-sulfur formation. Also, it is unclear whether and, if so, under what conditions the β-sulfur transforms into the orthorhombic phase. Considering the differences in density among both allotropes, such a solid–solid conversion would most likely have a strong and negative effect on the cycling performance. Overall, we believe that a comprehensive understanding of the structural changes during galvanostatic cycling will help develop future sulfur cathodes with improved properties.

4. Conclusions

In summary, we have shown that commercially available carbon blacks and poly(vinyl alcohol) Selvol 425 are suited to achieve the required conductive backbone structure in sulfur cathodes with a sulfur content of 60% and loadings of up to 2.3 $mg_{(S)}$ cm^{-2}. Our standardized system is well capable of competing in terms of sulfur utilization, cycling performance and other key parameters with the many nanostructured composite electrodes described in the literature, despite the simple cathode design. The results indicate that the sulfur distribution in the electrode and the rate capability are the limiting factors. However, these cathode-related issues are minor compared to both the apparent drying-out effects due to continuous electrolyte decomposition on the lithium metal anode and the high solubility of the generated polysulfides, particularly at elevated temperatures. In the long term, these latter issues inevitably result in cell failure and can probably only be resolved by introducing novel approaches in anode protection, as they are not directly related to the cathode architecture. Lastly, *in operando* X-ray diffraction demonstrates the formation of nanocrystalline Li_2S on discharge and single phase β-sulfur on charge. These data shed more light on the structural evolution of the active sulfur during cycling, but also bring up new questions.

Acknowledgements

We thank Christoph Weidmann, Artur Schneider, Sven Glatthaar, Lea de Biasi, Stephen Doyle and Holger Gesswein for assistance with the synchrotron-based XRD measurements. We acknowledge the Synchrotron Light Source ANKA for provision of beamtime at the PDIFF beamline. This study is part of projects being funded within the BASF International Network for Batteries and Electrochemistry.

Notes and references

1 X. Ji, K. T. Lee and L. F. Nazar, *Nat. Mater.*, 2009, **8**, 500.
2 X. Ji and L. F. Nazar, *J. Mater. Chem.*, 2010, **20**, 9821.
3 Y. V. Mikhaylik, I. Kovalev, R. Schock, K. Kumaresan, J. Xu and J. Affinito, *ECS Trans.*, 2010, **25**, 23.
4 B. L. Ellis, K. T. Lee and L. F. Nazar, *Chem. Mater.*, 2010, **22**, 691.
5 Z. Wei Seh, X. Li, J. J. Cha, G. Zheng, Y. Yang, M. T. McDowell, P.-C. Hsu and Y. Cui, *Nat. Commun.*, 2013, **4**, 1331.
6 S. S. Zhang, *J. Power Sources*, 2013, **231**, 153.
7 M. S. Whittingham, *Chem. Rev.*, 2004, **104**, 4271.
8 M. Armand and J.-M. Tarascon, *Nature*, 2008, **451**, 652.
9 D. Aurbach, E. Pollak, R. Elazari, G. Salitra, C. S. Kelley and J. Affinito, *J. Electrochem. Soc.*, 2009, **156**, A694.
10 M. R. Busche, P. Adelhelm, H. Sommer, H. Schneider, K. Leitner and J. Janek, *J. Power Sources*, 2014, **259**, 289.
11 Y. V. Mikhaylik and J. R. Akridge, *J. Electrochem. Soc.*, 2004, **151**, A1969.
12 C. D. Liang, N. J. Dudney and J. Y. Howe, *Chem. Mater.*, 2009, **21**, 4724.
13 X. Ji, S. Evers, R. Black and L. F. Nazar, *Nat. Commun.*, 2011, **2**, 325.
14 R. Demir-Cakan, M. Morcrette, F. Nouar, C. Davoisne, T. Devic, D. Gonbeau, R. Dominko, C. Serre, G. Férey and J.-M. Tarascon, *J. Am. Chem. Soc.*, 2011, **133**, 16154.
15 S. Jeong, D. Bresser, D. Buchholz, M. Winter and S. Passerini, *J. Power Sources*, 2013, **235**, 220.
16 S.-C. Han, M.-S. Song, H. Lee, H.-S. Kim, H.-J. Ahn and J.-Y. Lee, *J. Electrochem. Soc.*, 2003, **150**, A889.
17 W. Wei, J. Wang, L. Zhou, J. Yang, B. Schumann and Y. Nuli, *Electrochem. Commun.*, 2011, **13**, 399.
18 L. Yuan, H. Yuan, X. Qiu, L. Chen and W. Zhu, *J. Power Sources*, 2009, **189**, 1141.
19 L. Ji, M. Rao, S. Aloni, L. Wang, E. J. Cairns and Y. Zhang, *Energy Environ. Sci.*, 2011, **4**, 5053.
20 R. Elazari, G. Salitra, A. Garsuch, A. Panchenko and D. Aurbach, *Adv. Mater.*, 2011, **23**, 5641.
21 G. Zheng, Q. Zhang, J. J. Cha, Y. Yang, W. Li, Z. W. Seh and Y. Cui, *Nano Lett.*, 2013, **13**, 1266.
22 G. Zheng, Y. Yang, J. J. Cha, S. S. Hong and Y. Cui, *Nano Lett.*, 2011, **11**, 4462.
23 L. H. Yu, N. Brun, K. Sakaushi, J. Eckert and M. M. Titirici, *Carbon*, 2013, **61**, 245.
24 S. Dorfler, M. Hagen, H. Althues, J. Tubke, S. Kaskel and M. J. Hoffmann, *Chem. Commun.*, 2012, **48**, 4097.
25 J. Schuster, G. He, B. Mandlmeier, T. Yim, K. T. Lee, T. Bein and L. F. Nazar, *Angew. Chem., Int. Ed.*, 2012, **51**, 3591.
26 J. Wang, J. Yang, C. Wan, K. Du, J. Xie and N. Xu, *Adv. Funct. Mater.*, 2003, **13**, 487.
27 H. Wang, Y. Yang, Y. Liang, J. T. Robinson, Y. Li, A. Jackson, Y. Cui and H. Dai, *Nano Lett.*, 2011, **11**, 2644.

28 F. Wu, J. Chen, R. Chen, S. Wu, L. Li, S. Chen and T. Zhao, *J. Phys. Chem. C*, 2011, **115**, 6057.
29 S. Urbonaite and P. Novak, *J. Power Sources*, 2014, **249**, 497.
30 X. Liang, Z. Wen, Y. Liu, M. Wu, J. Jin, H. Zhang and X. Wu, *J. Power Sources*, 2011, **196**, 9839.
31 S. Xiong, K. Xie, Y. Diao and X. Hong, *Electrochim. Acta*, 2012, **83**, 78.
32 S. S. Zhang and J. A. Read, *J. Power Sources*, 2012, **200**, 77.
33 Y. V. Mikhaylik, Electrolytes for Lithium Sulfur Cells, *US Pat.*, 2011059350 A1, 2008.
34 C. Erk, T. Brezesinski, H. Sommer, R. Schneider and J. Janek, *ACS Appl. Mater. Interfaces*, 2013, **5**, 7299.
35 C. T. S. Campbell, J. Affinito and T. E. Kelley, Porous Structures for Energy Storage Devices, *US Pat.*, 20110206992 A1, 2011.
36 Y. Mikhaylik and K. Kumaresan, Cathode for Lithium Battery, *US Pat.*, 2010239914 A1, 2010.
37 W. F. Wilkening, C. T. S. Campbell and S. V. Burnside, Electrochemical Cells Comprising Porous Structures Comprising Sulfur, *US Pat.*, 2011059361 A1, 2011.
38 Y. Wang, Z. Xu, J. Affinito and C. D. Skaggs, Primer for a Battery Electrode, *US Pat.*, 2010291442 A1, 2010.
39 J. Zheng, D. Lv, M. Gu, C. Wang, J. G. Zhang, J. Liu and J. Xiao, *J. Electrochem. Soc.*, 2013, **160**, A2288.
40 Y. V. Mikhaylik and J. R. Akridge, *J. Electrochem. Soc.*, 2003, **150**, A306.
41 T. Xu, J. Song, M. L. Gordin, H. Sohn, Z. Yu, S. Chen and D. Wang, *ACS Appl. Mater. Interfaces*, 2013, **5**, 11355.
42 S. Walus, C. Barchasz, J. F. Colin, J. F. Martin, E. Elkaim, J. C. Lepretre and F. Alloin, *Chem. Commun.*, 2013, **49**, 7899.
43 J. Nelson, S. Misra, Y. Yang, A. Jackson, Y. Liu, H. Wang, H. Dai, J. C. Andrews, Y. Cui and M. F. Toney, *J. Am. Chem. Soc.*, 2012, **134**, 6337.
44 N. A. Canas, S. Wolf, N. Wagner and K. A. Friedrich, *J. Power Sources*, 2013, **226**, 313.